Dimerization of Fibril-forming Segments of α-Synuclein

Jeseong Yoon, Soonmin Jang,† Kyunghee Lee,† and Seokmin Shin*

*School of Chemistry, Seoul National University, Seoul 151-747, Korea. *E-mail: sshin@snu.ac.kr*
†Department of Chemistry, Sejong University, Seoul 143-747, Korea
Received June 03, 2009, Accepted June 18, 2009

We have performed replica-exchange molecular dynamics (REMD) simulations on the dimer formation of fibril-forming segments of α-Synuclein (residues 71 - 82) using implicit solvation models with two kinds of force fields-AMBER parm99SB and parm96. We observed spontaneous formation of dimers from the extensive simulations, demonstrating the self-aggregating and fibril forming properties of the peptides. Secondary structure profile and clustering analysis showed that dimers with antiparallel β-sheet conformations, stabilized by well-defined hydrogen boding, are major species corresponding to global free energy minimum. Parallel dimers with partial β-sheets are found to be off-pathway intermediates. The relative instability of the parallel arrangements is due to the repulsive interactions between bulky and polar side chains as well as weaker backbone hydrogen bonds.

Key Words: α-Synuclein, Replica-exchange molecular dynamics (REMD), Fibril formation, Antiparallel β-sheet

Introduction

Neurodegenerative diseases including Alzheimer's, Creutzfeldt-Jacob, and Parkinson's disease are associated with amyloid-like fibrils formed at neuronal surface.[1,2] Pathologies of these diseases, especially the mechanism of formation of oligomers or fibrils has been of great interests and extensive experimental researches have been performed.[3,4] Despite substantial advances in experimental studies, detailed information concerning atomic level features of structures and formation mechanism of protein aggregates are rather limited. In part, this is due to the non-crystalline and insoluble nature of amyloid fibrils. More importantly, corresponding proteins are intrinsically unstructured and exhibit noticeable conformational plasticity, which is highly sensitive to environmental conditions.[5] The characteristics of the so-called "intrinsically unstructured" or "intrinsically disordered" proteins have been actively investigated in recent years.[6-8] It has been gradually recognized that study of unfolded or partially folded states of natively or intrinsically unstructured proteins are essential to understanding some biological processes. Owing to remarkable increases in computational resources and developments in computational algorithms, one of the most direct and prominent theoretical approaches to investigate the structures and dynamics of protein misfolding and aggregation on molecular level is to perform systematic molecular dynamics simulations.[9] Computational studies provide an integral part of multidisciplinary approaches for elucidating various amyloid assemblies.[10]

A number of recent observations implicate α-synuclein in the pathogenesis of Parkinson's disease (PD).[11] In particular, the fibril formed from α-synuclein is the primary component of diagnostic hallmarks of PD such as Lewy bodies (LBs) and Lewy neuritis (LNs).[12-14] α-Synuclein is a 140 residue protein primarily found in neural tissue, especially in presynaptic terminals. It has been suggested that α-synuclein plays an important role in the pathogenesis of several neurodegenerative disorders. Circular dichroism (CD) and other optical methods showed that α-synuclein did not appear to possess a well-defined native structure, indicating its intrinsically unstructured nature.[15,16] α-Synuclein also exhibits a remarkable conformational plasticity depending on its environmental conditions.[17] The flexible structure of α-synuclein makes it versatile for its interaction with other proteins.[18] α-synuclein was shown to adopt mostly helical structure upon association with small unilamellar vesicles or detergent micelle surfaces.[19] It is reported that the region called non-amyloid component (NAC) corresponding to 61-95 amino acid sequence of human α-Synuclein plays a crucial role in fibril formation.[20] In the previous work, we examined conformational characteristics of the NAC region by replica exchange molecular dynamics simulations.[21,22]

Recently, experimental results suggest that a hydrophobic stretch of 12 amino acid residues in the middle of the NAC region is essential for filament assembly. The 71-82 sequence of α-synuclein is the main component of NAC sequence of α-synuclein and strongly hydrophobic. It is also noted that this 12 residue sequence of peptides can self-aggregate and form a fibril showing a β-sheet like CD spectrum.[23] The same region was predicted to be "aggregation-susceptible" with a high intrinsic propensity for aggregation.[24] In this work, we have performed replica-exchange molecular dynamics simulations on a pair of peptides corresponding to the 71-82 sequence in α-synuclein in order to investigate dimerization process and structural features of dimeric aggregates. The present study is expected to provide structural information on the first step of the self-aggregation process at molecular level.

Model and Simulation Details

Oligomerization process of a peptide involves orientational rearrangement and conformational change. One needs to use computational schemes based on efficient conformational sampling or relevant conformational constraints in order to describe such aggregation process in a reasonable computation time. REMD simulation has been performed as an efficient sampling

scheme for processes involving complex biomolecules.[25] In an attempt to observe the spontaneous ordering of oligomers, we have performed the replica exchange molecular dynamics (REMD) simulation for fibril-forming peptides of α-synuclein. To perform simulation process, linear chain of α-synuclein$_{(71-82)}$ sequence (VTGVTAVAQKTV) is prepared and copied to build a dimer. Initially, each peptide is randomly placed inside the simulation box. Peptides are confined within an imaginary sphere such that if the atoms are beyond the given boundary distance from the center of mass of the system, the attracting harmonic force centered at that boundary position will prohibit the molecules from flying apart from each other. The radius was chosen to be 30 Å, which was found to allow each peptide to move freely inside the sphere without severely disturbing the motion of the other peptide. After minimization process, the system is heated up to 500 K for 300 ps in order to obtain initial coordinates with randomly distributed conformations. At the next step, normal molecular dynamics simulation is performed for 500 ps on each replica without exchange, to equilibrate each replica at each corresponding temperature. REM simulation is performed with 16 replicas. The temperature distribution of REM includes 290, 300, 310.7, 322.1, 334.2, 347, 360.5, 374.7, 389.6, 405.2, 421.5, 438.5, 456.2, 474.6, 493.7, and 513.5 K. Exchange interval is every 200 steps (0.4 ps) and coordinates are recorded every 0.4 ps for further analysis. The exchange ratio is found to be ~25%. Simulations have been carried out using AMBER.[26] We have used two sets of force fields. First, the combination of AMBER parm99SB force field and the implicit solvation model by Mongan, *et al.*[27] was used. This solvation model employs an approximation of a molecular surface dielectric boundary so that it eliminates interstitial regions of high dielectric smaller than a solvent molecule. We also adopted the AMBER parm96 force field with the implicit solvation model by Onufriev, Bashford, and Case.[28] This solvation model is a modified Generalized-Born model in which the effective Born radii are re-scaled to account for the interstitial spaces between atom spheres missed in previous model, being intended to be a closer approximation to true molecular volume. The second combination was shown to be the most consistent in capturing the behavior of various peptides with balance between strand and helical conformations.[29] Periodic boundary conditions were used and the cut-off distance was 20 Å. The SHAKE algorithm[30] was used for bond constraints and the time step was 2 fs for all simulations. Total REM simulation time is 520 ns for parm96 force field and 1.04 μs for parm99SB force field. Most analyses including secondary structure calculations, radius of gyrations, clustering analysis, and principle component calculations are carried out using analysis modules in AMBER. All the results presented have been obtained from 300 K data.

Results and Discussion

The new version of AMBER parm99, called parm99SB, was designed to provide better balance between extended and helical conformations, overcoming an inaccurate representation of glycine and a strong α-helical emphasis in the original version.[27] However, parm99SB was found to be problematic in representing extended conformations and showed tendency to form helical structures with the use of the implicit salvation model of Onufriev, Bashford, and Case. On the other hand, the combination of AMBER parm99SB force field and the implicit solvation model by Mongan, *et al*. was reported to give a balanced conformation between extended and helical conformations.[31] We tested this combination of force fields on dimer simulations for fibril-forming peptides of α-synuclein. REMD simulation was performed for about 1 μs. To measure the degree of convergence, principle component analysis was done and the first two major principle component vectors were calculated. Simulation trajectory was projected to two-dimension space with these two major PC vectors as a basis. The projected PC space is divided by 50 × 50 grids between maximum and minimum values of projected trajectory coordinates. The time evolution of the number of visited grids is plotted as shown in Fig. 1. It was suggested that this method is useful in measuring the convergence of REMD simulation data.[32] It is noted that simulation trajectory seems to converge after about 170 ns. However, there exists a slight shift around 500 ns before it remains constant at somewhat different value. This result may suggest a possible structural transition at 500 ns. To examine the behavior of conformational properties, we calculated the time evolution of secondary structure content for the whole trajectory (Fig. 2). It is apparent that the dominant component is turn structure, while helix structures appear at the early stage before converging to a range of ~5% content after 500 ns. Concurrent with sudden decrease of helix contents, antiparallel β-sheet content increases and maintains a steady value, while the initial population of parallel β-sheet content also disappears after 500 ns. These results suggest that two peptides are initially aggregated into metastable conformations having partial helical structures and parallel β-sheets. The system seemed to be trapped in this state for rather long times before leading to more stable structure by proper rearrangement of the two peptides. During these structural transformations, unfavorable parallel arrangement is converted into antiparallel configuration which is expected to be energetically favorable.

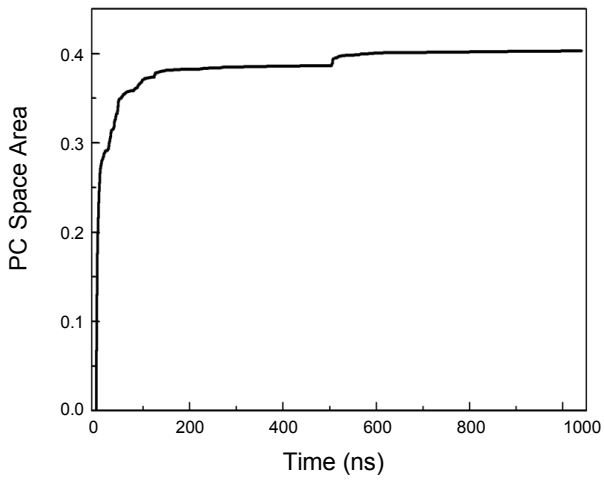

Figure 1. Time evolutions of the areas in PC space covered by simulation trajectories of dimer simulations for residues 71-82 of α-synuclein with the AMBER parm99SB force field. Vertical axis is the visited PC space area (× 10^4 Å^2).

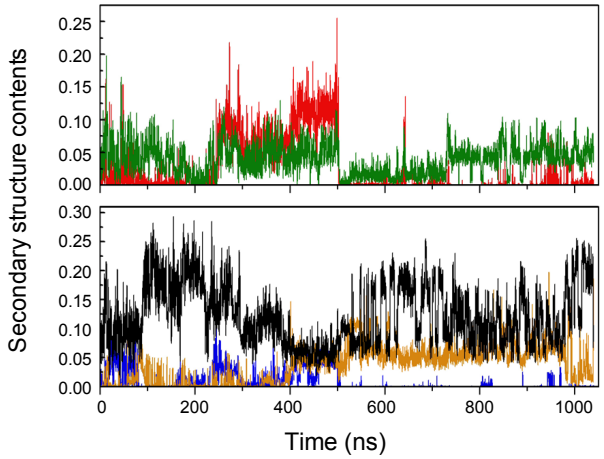

Figure 2. Time evolutions of the secondary structure contents from simulation trajectories of dimer simulations for residues 71-82 of α-synuclein with the AMBER parm99SB force field. Secondary structures are drawn in different colors: α-helix (red), 3_{10}-helix (green), antiparallel β-sheet (yellow), parallel β-sheet (blue), and turn (black).

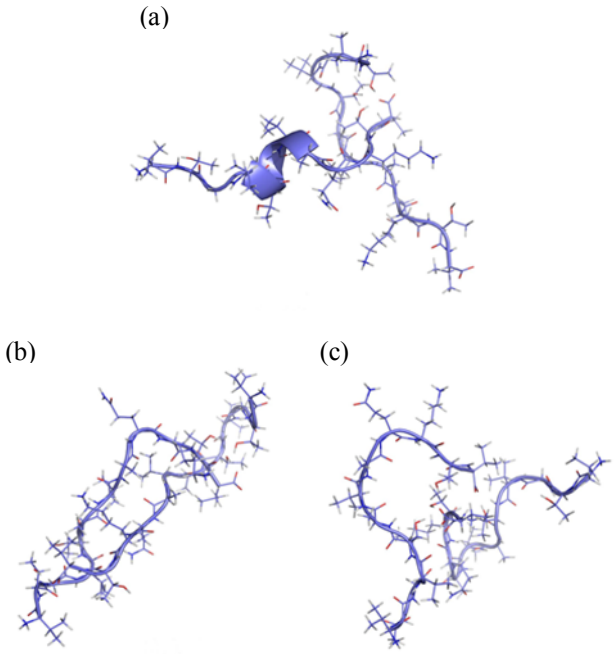

Figure 3. Three major dimer conformers from REMD simulations of two copies of peptides from the residues 71-82 of α-synuclein with the AMBER parm99SB force field.

Fig. 3 shows the representative conformers of dimers obtained from the clustering analysis on the last 10 ns trajectory. Clustering was done using K-means algorithm with RMS as distance metric. The conformation in the middle of the figure shows typical antiparallel arrangement, while the other two conformers are rather disordered. The lack of well-defined extended structure is likely to be the effects of parm99SB force field as mentioned before. Nevertheless, our results illustrate the possibility of stable dimer formation with antiparallel β-sheet conformation.

It was known that AMBER parm96 force field yield a rather high β strand propensity. Recent study claimed that the combination of AMBER parm96 force field and the implicit

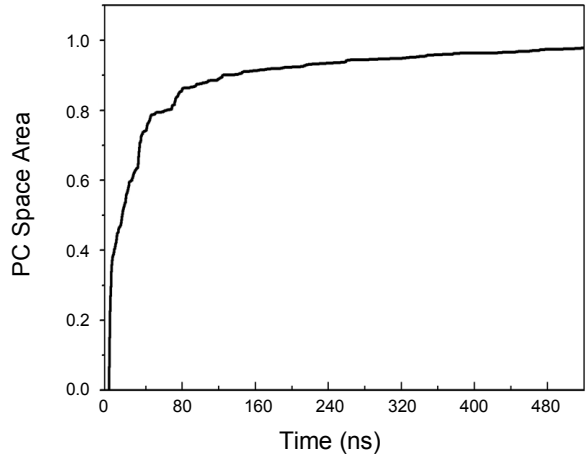

Figure 4. Time evolutions of the areas in PC space covered by simulation trajectories of dimer simulations for residues 71-82 of α-synuclein with the AMBER parm96 force field. Vertical axis is the visited PC space area ($\times 10^4$ Å^2).

solvation model by Onufriev, Bashford, and Case shows the most consistent results with the behaviors of several peptides of different conformational features and represents the extended conformational peptides well.[31] We adopted this combination of force fields on dimer simulation for fibril-forming peptides of α-synuclein. Convergence test showed that the convergence in PC space is achieved after 120 ns, which is faster than simulation trajectory with parm99SB (Fig. 4). The secondary structure contents showed that antiparallel β-sheet conformations are the most dominant species whenever dimers are formed (Fig. 5(a)). Time evolution of radius of gyration illustrates inter-conversion between dimer and monomer conformations (Fig. 5(b)): sharp peaks represent the break-up of a dimer to form monomers while the rapid reduction of R_g corresponds to the formation of dimers. The conformational diversity of dimers and coexisting monomers is demonstrated by different conformers obtained from the clustering analysis on the last 10 ns trajectory (Fig. 6). The monomer conformers and dimer conformations having partial parallel β-sheets or tail-to-tail aggregation with local antiparallel β-sheet bonds, are minor species, which can be considered as intermediate structures. There are two dominant antiparallel β-sheet conformational dimers with well-defined backbone hydrogen bond formation (conformers (b) and (g) in Fig. 6). In fact, about 70% of the conformational ensemble corresponds to well-arranged antiparallel β-sheet conformations. It is noted that one of the dimer conformations observed in parm99SB simulations (conformer (b) in Fig. 3) has the similar relative arrangements of residues in two chains as well as overall antiparallel geometry when compared with the two major conformers from the parm96 simulations. By performing the same clustering analysis on the other temperatures, it is also found that the stability of antiparallel conformations decreases as temperature increases: populations of antiparallel dimeric conformations at 290 K, 300 K, 310.7 K, and 322.1 K are 97%, 70%, 25%, and ~0%, respectively.

In order to characterize the structural properties of the two major conformations, we obtained C_α-C_α contact maps and

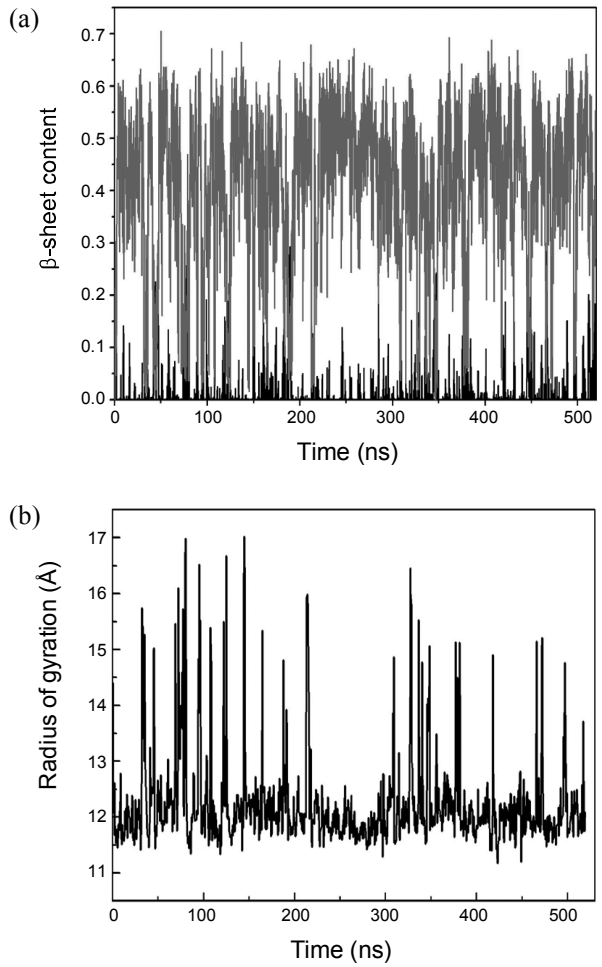

Figure 5. Time evolutions of (a) secondary structure contents and (b) radius of gyration for dimer simulations for residues 71-82 of α-synuclein with the AMBER parm96 force field. Antiparallel β-sheet is denoted by gray line and parallel β-sheet by black line in (a).

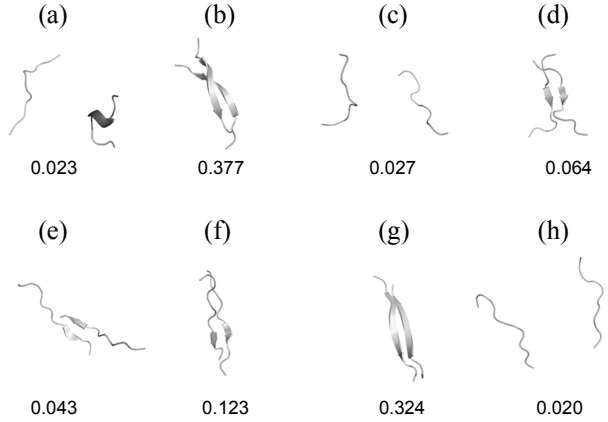

Figure 6. Various dimer conformers from REMD simulations of two copies of peptides from the residues 71-82 of α-synuclein with the AMBER parm96 force field. The numbers represent relative populations of different conformers.

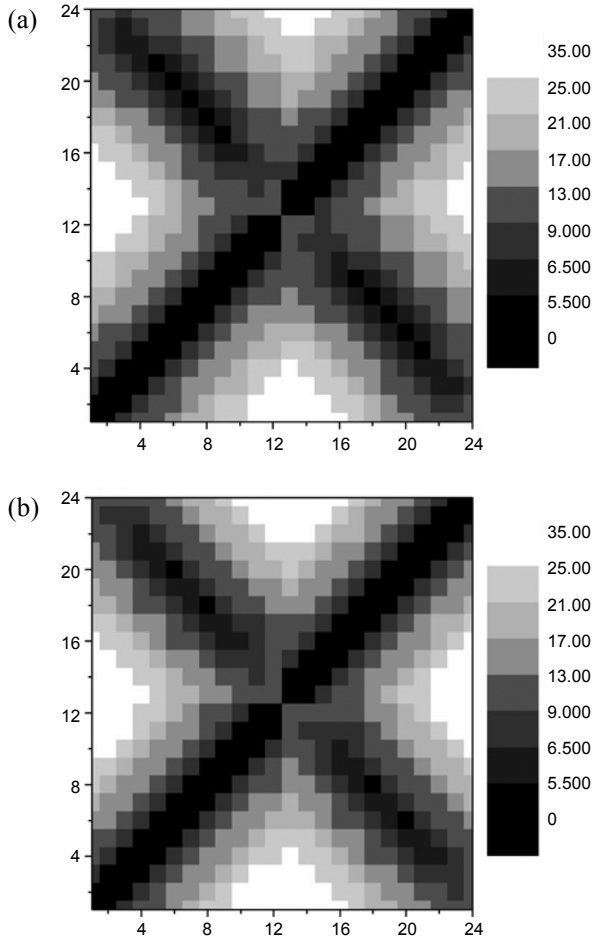

Figure 7. C_α-C_α contact maps for the two main conformers of the dimer: conformations (b) and (g) in Figure 6. Residue number corresponds to the concatenated index for the residues of the dimer.

calculated secondary structure content and root-mean-square atomic fluctuation for each residue. The results for C_α-C_α contact map showed that the two structures represent well-ordered antiparallel β-sheets with essentially the same register of backbone hydrogen bonds (Fig. 7). The structural similarities of the two major conformers are also illustrated by the distributions of the secondary structure contents and the atomic fluctuations as a function of the residue along the corresponding chains (Fig. 8). As expected, the region with well-defined backbone hydrogen bonds corresponds to low backbone atomic fluctuations. Fig. 9 shows the backbone representative structures for the two major conformations and the schematic diagram of β-sheet registry consistent with the common configuration.

We calculated a free energy surface as a function of the two main principle components using the simulation trajectory of the last 120 ns (Fig. 10). Various conformations obtained from the cluster analysis described above are placed at the corresponding positions in the PC space. These conformers can be grouped into three species: two separated monomers, partial parallel β-sheets, and antiparallel β-sheets, which comprise different regions of the free energy space as indicated in the figure. It is clearly shown that antiparallel β-sheet conformational dimers represent global minium region in the free energy, while parallel dimers with partial β-sheets are relatively unstable intermediates. It is seen that the representative structures of clusters (b), (e), and (g) with antiparallel β-sheet conformations are not exactly located at the global minimum (dark

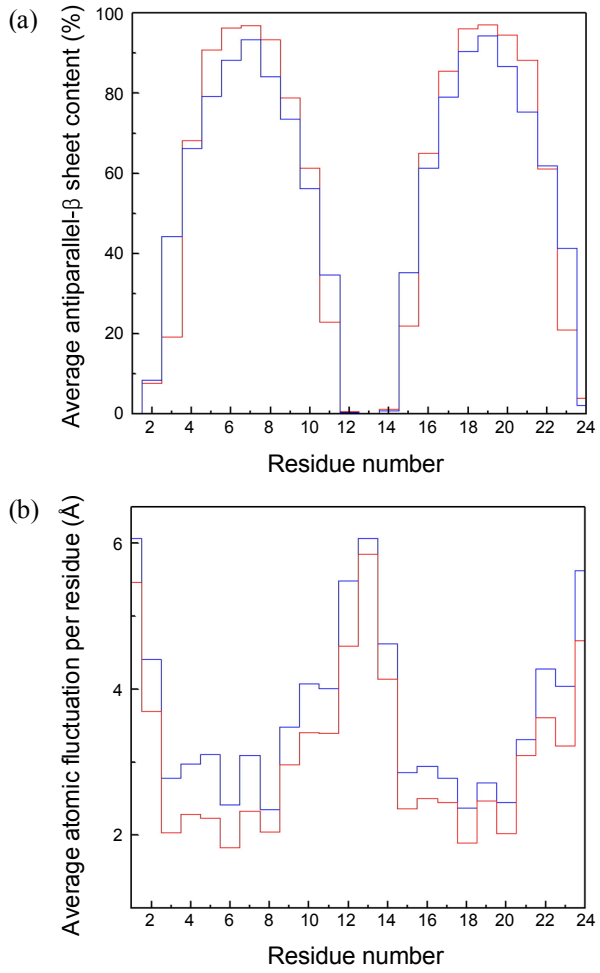

Figure 8. (a) Average antiparallel β-sheet contents and (b) average atomic root mean square fluctuations as a function of residue along the chains for the two main conformers of the dimer: conformations (b) (red line) and (g) (blue line) in Figure 6. Residue number corresponds to the concatenated index for the residues of the dimer.

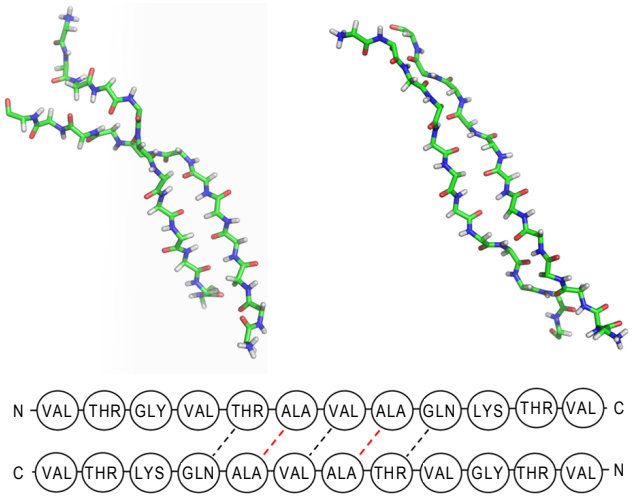

Figure 9. Backbone representative structures for the two main conformers of the dimer: conformations (b) and (g) in Figure 6. Also shown is the schematic registry of the antiparallel β-sheet configuration common for the two conformations. Dashed lines represent well-defined hydrogen bonding with the red lines denoting the closest bonds.

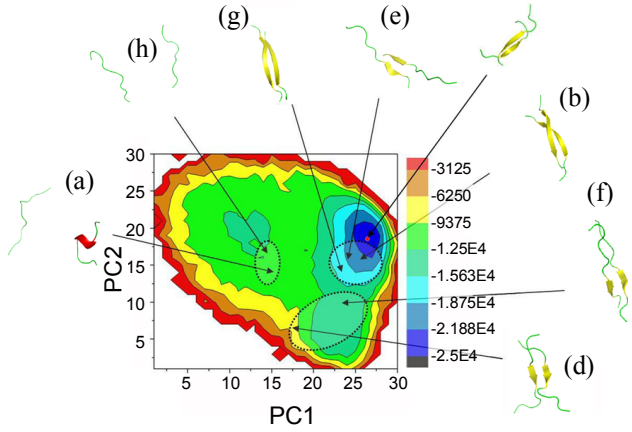

Figure 10. Free energy surface as a function of the two main principle components obtained from the trajectory of the last 120 ns for dimer simulations for residues 71-82 of α-synuclein with the AMBER parm96 force field. Unit of energy shown in scaling bar is J·mol^{-1}. Various conformers shown in Figure 6 are located at the corresponding positions in PC space. One of the structures in cluster (b) corresponding to the middle of global minimum region is also shown.

blue region). This is due to the fact that the representative structure is not the centroid structure of that cluster, but the available structure closest to the centroid structure. In fact, the mean position of 9413 structures of cluster (b) is located at (PC1, PC2) = (27, 17) and corresponds to global minimum region. One of the structures in cluster (b) corresponding to the middle of global minimum region is also shown in Fig.10. One can deduce the aggregation mechanism of dimer formation as follows. As the two chains get closer due to favorable hydrophobic interactions, they can adopt two orientations: parallel or antiparallel arrangements. For parallel dimers, even though they can form partial β-sheets with few hydrogen bonds, the resulting structure is relatively unstable and may disintegrate easily. For antiparallel dimers, the intermediate structures with partial hydrogen bonds are relatively stable and can be extended to form more stable antiparallel β-sheets with well-defined hydrogen bonding patterns.

Concluding Remarks

We have performed replica-exchange molecular dynamics (REMD) simulations on the dimer formation of fibril-forming segments of α-synuclein (residues 71-82) using implicit solvation models with two kinds of force fields-AMBER parm99SB and parm96. We observed spontaneous formation of dimers from the extensive simulations. Secondary structure profile and clustering analysis showed that dimers with antiparallel β-sheet conformations, stabilized by well-defined hydrogen boding, are major species corresponding to global free energy minimum. Parallel dimers with partial β-sheets are found to be off-pathway intermediates. The relative instability of the parallel arrangements is due to the repulsive interactions between bulky and polar side chains as well as weaker backbone hydrogen bonds than antiparallel hydrogen bonds. For small peptides, repulsions due to steric and Coulombic interactions

between the same residues are dominant such that antiparallel arrangements are relatively stable. It can be argued that these results may be generalized to aggregation processes of short peptide oligomers regardless of their specific sequences. Further investigations on the aggregation of higher oligomeric species of small peptides and oligomers of longer sequences will give useful information on the structural diversity and dynamical heterogeneity of oligomerization processes.

Acknowledgments. This work was supported by grant R01-2006-000-10418-0 from the Basic Research Program of the Korea Science & Engineering Foundation. This work was also supported by the Korea Science & Engineering Foundation through the Center for Space-Time Molecular Dynamics (2008).

References

1. Dobson, C. M. *Nature* **2003**, *426*, 884.
2. Ross, C. A.; Poirier, M. A. *Nat. Med.* **2004**, *10*, S10.
3. Skovronsky, D. M.; Lee, V. M.-Y.; Trojanowski, J. Q. *Annu. Rev. Pathol. Mech. Dis.* **2006**, *1*, 151.
4. Chiti, F.; Dobson, C. M. *Annu. Rev. Biochem.* **2006**, *75*, 333.
5. Fink, A. *Acc. Chem. Res.* **2006**, *39*, 628.
6. Uversky, V. N.; Oldfield, C. J.; Dunker, A. K. *Annu. Rev. Biophys.* **2008**, *37*, 215.
7. Dunker, A. K.; Lawson, J. D.; Brown, C. J.; Williams, R. M.; Romero, P.; Oh, J. S.; Oldfield, C. J.; Campen, A. M.; Ratliff, C. M.; Hipps, K. W.; Ausio, J.; Nissen, M. S.; Reeves, R.; Kang, C.; Kissinger, C. R.; Bailey, R. W.; Griswold, M. D.; Chiu, W.; Garner, E. C.; Obradovic, Z. *J. Mol. Graph. Modell.* **2001**, *19*, 26.
8. Uversky, V. *Prot. Sci.* **2002**, *11*, 739.
9. Ma, B.; Nussinov, R. *Curr. Opin. Chem. Biol.* **2006**, *10*, 445.
10. Teplow, D. B.; Lazo, N. D.; Bitan, G.; Bernstein, S.; Wyttenbach, T.; Bowers, M. T.; Baumketner, A.; Shea, J. E.; Urbanc, B.; Cruz, L.; Borreguero, J.; Stanley, H. E. *Acc. Chem. Res.* **2006**, *39*, 635.
11. Lücking, C. B.; Brice, A. *Cell. Mol. Life. Sci.* **2000**, *57*, 1894.
12. Spillantini, M. G.; Schmidt, M. L.; Lee, V. M.; Trojanowski, J. Q.; Jakes, R.; Goedert, M. *Nature* **2006**, *388*, 839.
13. Shults, C. W. *Proc. Natl. Acad. Sci. USA* **2006**, *103*, 1661.
14. Kim, S.; Seo, J.; Suh, Y. *Park. Rel. Dis.* **2004**, *10*, S9.
15. Eliezer, D.; Kutluay, E.; Bussell, Jr., R.; Browne, G. *J. Mol. Biol.* **2001**, *307*, 1061.
16. Uversky, V. N.; Li, J.; Fink, A. L. *J. Biol. Chem.* **2001**, *276*, 10737.
17. Uversky, V. N. *J. Biomol. Struct. Dyn.* **2003**, *21*, 211.
18. Lee, I.-H.; Kim, H. J.; Lee, C.-H.; Paik, S. R. *Bull. Kor. Chem. Soc.* **2006**, *27*, 1001.
19. Ulmer, T. S.; Bax, A.; Cole, N. B.; Nussbaum, R. L. *J. Biol. Chem.* **2005**, *280*, 9595.
20. Iwai, A. I.; Yoshimoto, M.; Masliah, E.; Saitoh, T. *Biochemistry* **1995**, *34*, 10139.
21. Yoon, J.; Park, J.; Jang, S.; Lee, K.; Shin, S. *J. Biomol. Struct. Dyn.* **2008**, *25*, 505.
22. Yoon, J.; Park, J.; Jang, S.; Lee, K.; Shin, S. *Bull. Kor. Chem. Soc.* **2009**, *30*, 623.
23. Giasson, B. I.; Murray, I. V. J.; Trojanowski, J. Q.; Lee, V. M.-Y. *J. Biol. Chem.* **2001**, *276*, 2380.
24. Pawar, A. P.; Dubay, K. F.; Zurdo, J.; Chiti, F.; Vendruscolo, M.; Dobson, C. M. *J. Mol. Biol.* **2005**, *350*, 379.
25. Sugita, Y.; Okamoto, Y. *Chem. Phys. Lett.* **1999**, *314*, 141.
26. Case, D. A.; Darden, T. A.; Cheatham, T. E. I.; Simmerling, C. L.; Wang, J.; Duke, R. E.; Luo, R.; Merz, K. M.; Wang, B.; Pearlman, D. A.; Crowley, M.; Brozell, S.; Tsui, V.; Gohlke, H.; Mongan, J.; Hornak, V.; Cui, G.; Beroza, P.; Schafmeister, C.; Caldwell, J. W.; Ross, W. S.; Kollman, P. A. *AMBER8 University of California, San Francisco,* 2004.
27. Mongan, J.; Simmerling, C.; McCammon, J. A.; Case, D. A.; Onufriev, A. *J. Chem. Theory Comput.* **2006**, *3*, 156.
28. Onufriev, A.; Bashford, D.; Case, D. A. *Proteins* **2004**, *55*, 383.
29. Shell, M. S.; Ritterson, R.; Dill, K. A. *J. Phys. Chem. B* **2008**, *112*, 6878.
30. Ryckaert, J. P.; Cicotti, G.; Berendsen, H. J. C. *J. Comput. Phys.* **1977**, *23*, 327.
31. Shell, M. S.; Ritterson, R.; Dill, K. A. *J. Phys. Chem. B* **2008**, *112*, 6878.
32. Zhang, W.; Wu, C.; Duan, Y. *J. Chem. Phys.* **2005**, *123*, 154105.